1   **Interpreting the ^{13}C/^{12}C ratio of carbon dioxide in an urban airshed in the Yangtze**
2   **River Delta, China**

4   Jiaping Xu[1], Xuhui Lee[1,2*], Wei Xiao[1], Chang Cao[1], Shoudong Liu[1], Xuefa Wen[3], Jingzheng
5   Xu[1], Zhen Zhang[1], Jiayu Zhao[1]

7   [1]Yale-NUIST Center on Atmospheric Environment, Nanjing University of Information
8   Science & Technology, Nanjing, China

10   [2]School of Forestry and Environmental Studies, Yale University, New Haven, Connecticut,
11   USA

13   [3]Key Laboratory of Ecosystem Network Observation and Modeling, Institute of Geographic
14   Sciences and Natural Resources Research, Chinese Academy of Sciences, Beijing, China

16   * Corresponding author
17   Dr. Xuhui Lee
18   Sara Shallenberger Brown Professor
19   School of Forestry and Environmental Studies, Yale University,
20   21 Sachem Street, New Haven, Connecticut 06510, USA
21   Phone: (203)432-6271; Fax: (203)432-5023
22   E-mail: xuhui.lee@yale.edu

24   **Abstract:** Observations of atmospheric CO_2 molar fraction and its ^{13}C isotope composition

25   ($\delta^{13}C$) in urban airsheds provide constraints on the roles of anthropogenic and natural sources

26   in local and regional C cycles. In this study, we report observations of these quantities in

27   Nanjing at hourly intervals from March 2013 to August 2015 using a laser-based optical

28   instrument. Nanjing is the second largest city located in the highly industrialized Yangtze

29   River Delta (YRD), Eastern China. The mean CO_2 molar fraction and ^{13}C were 439.7 ppm

30   and -8.48‰ over this observational period. The peak monthly mean $\delta^{13}C$ (-7.44‰, July 2013)

31   was 1.03‰ higher than that observed at the Mauna Loa Observatory. The highly enriched ^{13}C

32   signal was attributed to the influence of cement production in the region. By applying the

33   Keeling plot and the Miller-Tans method to midnight and midday observations, respectively,

34   we showed that the ^{13}C signal of C sources in the Nanjing Municipality was 0.48‰ lower

35   than that in the YRD. Flux partitioning calculations revealed that natural ecosystems in the

36   YRD were a negligibly small sink of atmospheric CO_2, consistent with the Carbon Tracker

37   inverse modeling result.

39   **Keywords:** urban areas; CO_2 flux; Industrial process; Carbon isotope; In-situ observation

1 Introduction

Atmospheric CO_2 sources in urban areas consist mainly of plant uptake and release and fossil

fuel combustion. These sources have their unique ^{13}C isotopic signatures. City clusters are

human-dominated systems with high carbon emission intensity, contributing over 70% of the

total anthropogenic CO_2 to the atmosphere (Satterthwaite 2008). Previous urban isotopic

studies emphasize carbon emissions from fossil combustion (Zondervan and Meijer 1996,

Pataki et al. 2003, Zimnoch et al. 2004, Affek and Eiler 2006, Newman et al. 2008).

Relatively little attention is given to the isotopic signature of carbon dioxide released by

cement production, which is much heavier than that of fossil fuel origin (Andres et al. 1994).

Likewise, the CO_2 emitted from burning of minerals in non-energy consumption industrial

processes, such as iron and steel production, has higher ^{13}C composition than that of fossil

(Table 1, Widory 2006). In China, cement production and industrial processes contribute 13%

of the total anthropogenic CO_2 emission (Mu et al. 2013). Many of these industrial activities

occur in or near urban areas. So far, little is known about their roles in the atmospheric $\delta^{13}C$

budget.

One scientific motivation for quantifying the ^{13}C signature of atmospheric CO_2 is that it

provides constraints that allow partitioning of the net surface flux into component fluxes

(Farquhar and Lloyd 1993, Yakir and ternberg 2000, Pataki et al. 2003). The ^{13}C-based

partitioning method has been used primarily for vegetation ecosystems, such as forests

(Lloyd et al. 1996, Lloyd et al. 2001, Ometto, et al. 2006, Zobitz et al. 2008), grasses (Ometto

et al. 2002, Pataki et al. 2003), and crops (Leavitt et al. 1995, Griffis et al. 2005). The

approach has also been used in a limited number of urban studies (Pataki et al. 2003,

63   Zimnoch et al. 2004, Newman et al. 2008, Jasek et al. 2014). Compared with vegetation

64   ecosystems, urban ecosystems have more complex CO_2 source configuration. We must

65   consider both natural sources (plants and soils) and anthropogenic sources (fossil combustion

66   and non-energy industrial processes) and the fact the degree of mixing of urban air with the

67   free troposphere and the air outside the urban boundary varies diurnally and seasonally.

68   Anthropogenic emissions are hard to quantity because they depend on multiple factors

69   including city size, population density, fossil mix, and climate.

70   One of the first measurements of the carbon isotope composition of CO_2 in an urban

71   atmosphere was made by Friedman and Irsa (1967). Since then, a few more experiments have

72   been conducted in urban environments. The data collected have been used to partition CO_2

73   contributors (Koerner and Klopatek 2002, Clark-Thorne and Yapp 2003), to quantify diurnal

74   variations in the CO_2 molar fraction and its $\delta^{13}C$ in urban air (Zimnoch et al. 2004, Guha and

75   Ghosh 2010) and across urban to rural gradients (Lichtfouse et al. 2003, Pataki et al. 2007),

76   and variations among different land uses in urban areas (Clark-Thorne and Yapp 2003,

77   Widory and Javoy 2003). The isotopic data reveals insights into energy consumption patterns

78   (Widory and Javoy 2003, Bush et al. 2007), impacts of meteorology including temperature

79   (Clark-Thorne and Yapp 2003, Zimnoch et al. 2004), atmospheric stability (Pataki et al. 2005)

80   and wind (Clark-Thorne and Yapp 2003) on urban carbon cycling, and the role of vegetation

81   phenology (Ehleringer et al. 2002, Takahashi et al. 2002, Wang and Pataki 2012). The

82   analytical technique deployed in these studies is mainly based on mass-spectrometry (MS).

83   Because sample collection, preparation and analysis are labor intensive, the majority of these

84   studies are limited to short campaigns (less than 60 days).

85   In recent years, the development of isotope ratio infrared spectroscopy (IRIS) and on-line

86   calibration technology provides a new solution for long-term in-situ observation of the CO_2

87   molar fraction and its $\delta^{13}C$ at high frequencies (1 Hz to 1 hour; Pataki et al. 2006, Griffis.

88   2013,   Gorski et al. 2015). Compared with the MS method, IRIS can capture diurnal or even

89   shorter temporal variations with relatively high accuracy, enabling us to understand how

90   anthropogenic emissions change atmopheric CO_2 at various temporal and spatial scales.

91   Nevertheless, application of the IRIS technology in urban monitoring is still limited in terms

92   of cities covered and measurement duration (less than 35 days; McManus et al. 2002, Pataki

93   et al. 2006, Wada et al. 2011; 3 seasons; Moore and Jacobson 2015) and only one published

94   study has presented data that spans one full annual cycle (Pang et al. 2016).

95   Simultaneous measurement of atmospheric CO_2 concentration and its isotopic

96   composition is used to determine the overall isotopic signature of local surface sources $\delta^{13}C_S$.

97   All published urban studies to date have deployed the Keeling plot method (Keeling 1958,

98   Keeling 1961) for the determination of $\delta^{13}C_S$. In this approach, a linear relationship is

99   established between $\delta^{13}C$ and the reciprocal of the CO_2 molar fraction from the observed time

100   series, and the intercept of the linear regression is taken as the isotopic composition of the

101   local CO_2 emissions. The method assumes that the isotopic signature of the sources is

102   invariant with time. It also assumes that changes in the CO_2 molar fraction and $\delta^{13}C$ are

103   attributed only to the surface sources and are unaffected by regional carbon sources (Pataki et

104   al. 2003). However, these assumptions strictly do not hold in an urban environment because

105   the intensity of traffic emissions varies strongly through the diurnal cycle (McDonald et al.

106   2014), and therefore the effective source ^{13}C signature cannot be assumed constant. In

107   addition, because of strong atmospheric mixing in the daytime convective boundary layer, the

108   background air in the upper troposphere can be easily entrained to the surface layer, mixing

109   the CO_2 that originates from regional sources with that emitted locally in the urban airshed.

110   Miller and Tans (2003) propose that $\delta^{13}C_S$ be determined as the slope of the linear

111   relationship

112     $$\delta_a C_a - \delta_b C_b = \delta^{13}C_s (C_a - C_b)$$ (1)

113   where C_a is CO_2 molar fraction in urban air, C_b is CO_2 molar fraction in a background site

114   [taken in this study as that observed at the Mauna Loa Observatory (MLO)], δ_a is ^{13}C isotopic

115   composition of C_a, and δ_b is ^{13}C isotopic composition of C_b. We argue that because this

116   approach takes into account mixing of CO_2 generated locally with CO_2 in the background

117   atmosphere, this method is more suitable than the Keeling method for inferring $\delta^{13}C_S$ from

118   the observations made in the daytime when such mixing occurs. The method has been applied

119   to local and regional carbon budget studies in nonurban settings (Miller et al. 2003). We are

120   not aware of studies that extend the method to an urban environment.

121   In this study, we report the results of long-term (30 months) continuous measurement of

122   atmospheric CO_2 molar fraction and its $\delta^{13}C$ at a suburban site in Nanjing using an IRIS

123   instrument. Nanjing is the second largest city in the Yangtze River Delta (YRD), Eastern

124   China, with a build-up area of 753 km^2 and a population of 8.2 million. Geographically, the

125   YRD include the provinces of Jiangsu, Zhejiang and Anhui and the Shanghai municipality.

126   The YRD is the most industrialized region in China and had a higher urban land fraction of

127   10.8% as of 2014 than the global mean (2.4%, Akbari et al. 2009). In 2014, more than 220

128   large cement production factories (daily output exceeding 1000 tons) were located in the

129   YRD, contributing about 20% of the national cement output.

130   Our objectives are (1) to characterize the atmospheric $\delta^{13}C$ diurnal, seasonal and annual

131   variations in this urban environment, in a region where such measurement is nonexistent, (2)

132   to investigate the influence of cement production on atmospheric $\delta^{13}C$, (3) to evaluate the

133   performance of the Keeling plot and the Miller-Tans method for determining $\delta^{13}C_S$, and (4) to

134   explore the utility of the isotopic constraints for inferring the net surface flux and the plant

135   CO_2 flux in Nanjing and in the YRD.

136

137   **2 Methods**

138   **2.1 Atmospheric observation**

139   An IRIS analyzer (model G1101-i, Picarro Inc., Sunnyvale, CA) was used to measure

140   atmospheric CO_2 molar fraction and its ^{13}C isotope composition ($\delta^{13}C$) continuously from

141   February 2013 to August 2015. The measurement was made at 0.3 Hz and at an air flow rate

142   of 30 mL min^{-1} at standard temperature and pressure. One three-way solenoid valve was

143   combined with two two-way solenoid valves, so the analyzer could be switched for

144   atmospheric sampling and for sampling of two standard gases. Calibration was carried out

145   every 3 h by sampling each standard gas for 5 minutes following the procedure of Bowling et

146   al. (2003) and Wen et al. (2013). Table 1 lists the concentrations and their isotopic

147   compositions of the standard gases used in this study. The CO_2 molar fraction of the standard

148   gases was traceable to the WMO 2007 scale reported by the Central Calibration Laboratory

149   of the World Meteorological Organization and their $\delta^{13}C$ was based on the NBS-19 and the

150   NBS20 standards of NOAA-EASL. The ambient measurement was averaged to hourly

151   intervals. The isotopic composition was expressed in the delta notation (δ^{13}C) in reference to

152   the VPDB scale.

153   The analyzer was housed on the 9th floor of our laboratory building on the campus of

154   Nanjing University of Information, Science and Technology (NUIST, 32°12'N, 118°43'E), in

155   the northern suburb of Nanjing, at a linear distance of 20 km to the city center. The

156   instrument inlet was at a height of 34 m above the ground. There was no anthropogenic CO_2

157   source in the 3 km radius except for a commuting road located about 300 m east of the

158   observation site. The nearest industrial complex, the Nanjing Iron & Steel Group Co. Lt and

159   the Nanjing Chemical Industry Group, was located at ~5 km to the south of the site.

160   The δ^{13}C measured by the analyzer in high humidity conditions suffers a high bias error

161   due to spectral broadening and direct spectral interference (Rella 2011). To correct for the

162   humidity interference, we carried out two tests using a dew-point generator (model 610, LI-

163   COR, Inc., Lincoln, NE). A CO_2 standard gas (secondary standard gas, 439 ppm in test one

164   and 488 ppm in test two, balanced by dry air) was fed into the dew-point generator. The

165   outlet of the dew-point generator was connected with a 3-way union with one end linked to

166   the inlet of the analyzer and the other open to the room. The humidity level of the air coming

167   out of the dew point generator was regulated at eight levels in a dew-point temperature range

168   of 1 and 30℃. Because the ^{13}C composition of the standard gas was constant, any observed

169   variations were caused by the humidity artifact. We found that no correction was needed for

170   our analyzer if the humidity was below 2.03%. Above this humidity level, the measurement

171   was biased high by 0.46‰ for every 1% increase in the water vapor volume molar fraction

172   (Figure 1). The two tests, taken eight months apart, yielded essentially the same result. The

173   correction equation is

174    $\delta^{13}C = \delta^{13}C_{true}$ $\qquad$ $H \leq 2.03\%$ $\qquad\qquad$ (2a)

175    $\delta^{13}C = \delta^{13}C_{true} + 0.46(H - 2.03)$ $\qquad$ $H > 2.03$ $\qquad\qquad$ (2b)

176   where H is water vapor volume molar fraction in percent, $\delta^{13}C$ is the measured isotopic

177   composition (after the two-point calibration), and $\delta^{13}C_{true}$ is the true isotopic composition. In

178   the following, all the data has been corrected for the humidity interference.

179

180   **2.2 The isotopic composition ($\delta^{13}C_S$) of surface sources**

181   We applied the Keeling plot method to the data collected during midnight hours (22:00-6:00

182   local time). We used the geometric regression to establish a linear relationship between the

183   hourly $\delta^{13}C$ and the reciprocal of the hourly CO_2 molar fraction over monthly intervals. The

184   intercept of the regression gives the effective isotopic composition of net surface CO_2

185   emissions. The buildup of CO_2 at night is primarily the result of sources in the city (Shen et

186   al. 2014), so we considered the $\delta^{13}C_S$ determined from the nighttime observations to represent

187   the signal of the sources located in the city.

188   We applied the Miller-Tans method to the data collected in midday hours (10:00 to 16:00

189   local time; Equation 1). The slope was obtained by linear regression of C_a against ($\delta_a C_a$-

190    $\delta_b C_b$), again over monthly intervals. The monthly mean CO_2 molar fraction and the isotopic

191   composition of the background air were those observed at MLO. Because the MLO data were

192   not available for 2015 at the time of this analysis, we first established a four-harmonic

193   quadratic function (Thoning et al. 1989) using the dataset from 2000 to 2013, and then used

194   the function to estimate the monthly $\delta^{13}C_b$ and C_b values for 2015. The vigorous turbulent

195   exchange in the midday boundary layer diminishes the role of local sources in the measured

196   concentration and isotopic ratio, or in other words, the midday measurement has a much

197   larger source footprint than the size of the urban land itself or the footprint of the midnight

198   measurement. Hence we interpreted the midday results to represent the influence of surface

199   sources in the YRD region. This interpretation is supported by a trajectory analysis and by an

200   analysis of the atmospheric methane to CO_2 emissions ratio (Shen et al. 2014).

201

202   **2.3 Inventory of anthropogenic sources**

203   We calculated the anthropogenic CO_2 fluxes from energy consumption and industrial process

204   following the scope one procedure issued by the International Council for Local

205   Environmental Initiatives (ICLEI, 2008). The energy consumption source consisted of direct

206   emissions from the three main energy consumption sectors (industry, transport, and

207   household). We ignored the commerce sector here because the main energy consumption in

208   this sector in Nanjing and in the YRD was electric power generated by coal and coal

209   consumption which was already considered in scope one. The amounts of CO_2 emission were

210   estimated with the IPCC methodology adopting the emission factors for each fossil fuel type

211   recommended by IPCC. The calculations were done for both the YRD region and for the

212   Nanjing municipality. Because no statistical data were available for energy consumption in

213   the transport sector in Nanjing, the CO_2 emission from the transport sector was deduced

214   according to vehicle number, average annual driving distance and coefficients of fuel

215   economy (Bi et al. 2011). We obtained the data on energy consumption from official sources

216   (CESY 2013, CSY 2013, NSY, 2013).

217   The non-energy industrial processes included cement, raw iron, crude steel, and

218   ammonia synthesis processes. In the YRD, the data were available at monthly intervals. For

219   the city of Nanjing, only annual statistics were available.

220

2.4 Partitioning the net surface flux

222   We partitioned net surface CO_2 flux (F_S) into three component fluxes according to the

223   following mass conservation equations

224    $$F_S = F_F + F_C + F_P \qquad\qquad (3)$$

225    $$\delta^{13}C_S F_S = \delta^{13}C_F F_F + \delta^{13}C_C F_C + \delta^{13}C_P F_P \qquad\qquad (4)$$

226   where F_F is the flux from fossil fuel combustion and industrial emission except cement

227   production (termed "fossil plus"), F_C is the flux due to cement production, F_P is the plant

228   flux, and $\delta^{13}C_F$, $\delta^{13}C_C$, and $\delta^{13}C_P$ are the ^{13}C isotope composition of F_F, F_C and F_P,

229   respectively. We separated the cement source from other non-energy consumption industrial

230   processes because its isotopic signature is much higher. In these equations, the monthly net

231   surface flux (F_S) and the plant flux (F_P) are unknowns to be solved, and all other terms are

232   either provided by the atmospheric measurement or by the inventory calculation. The

233   partitioning analysis was done for both Nanjing and the YRD using the midnight and midday

234   observations, respectively.

235   The $\delta^{13}C_F$ was weighted average of the $\delta^{13}C$ signal of individual fuel types and industrial

236   processes (Widory 2006; Table 1). The cement isotopic composition is provided by Tans

237   (1981) and Anders (1994). We adapt a value of (-28.2‰) for $\delta^{13}C_P$ for the YRD and Nanjing,

238   on account of a linear relationship between $\delta^{13}C_P$ and tree age (Fessenden and Ehleringer

239   2002), a typical tree age in this region (40 years) and an U-shaped relationship between $\delta^{13}C_P$

240   and annual precipitation (Pataki et al. 2007). Our $\delta^{13}C_P$ is more negative than that reported for

241   a boreal forest (-26.2‰; Pataki et al. 2007) but is in closer agreement with the value reported

242   for a Ginkgo tree in Nanjing (-29.3‰; Sun et al. 2003). A summary of the isotopic

243   compositions of the three source categories is given in Table 2.

244   To partition the nighttime flux for Nanjing, we assumed that the nighttime F_F was 20%

245   of the daily value. The parameter 20% was determined by the diurnal variation of the CO_2

246   flux observed with an eddy covariance system in Nanjing (Bai 2011) and in several other

247   cities (Coutts et al. 2007, Song and Wang. 2011, Liu et al. 2012). At night, most of the

248   factories in the city were closed and the traffic flow was reduced to about 80% of the daytime

249   volume (Yang et al. 2011).

250

251   **3. Results**

252   **3.1. Temporal variations in the CO_2 molar fraction and $\delta^{13}C$**

253   The monthly CO_2 molar fraction during the summer was slightly lower than in the other

254   seasons (Figure 2). The mean molar fraction was 446.7 ppm and 431.1 ppm for January and

255   July, respectively, giving a seasonal amplitude of 15.6 ppm. The mean CO_2 molar fraction

256   was 439.7 ppm during the whole experimental period (March 2013 to August 2015), which is

257   40.7 ppm higher than value observed at MLO for the same period. In 2014, the calendar year

258   with complete data coverage, the mean CO_2 molar fraction was 441.2 ppm, which is 42.5

259   ppm higher than the MLO value for the same year.

260   The ^{13}C composition of atmospheric CO_2 displayed a stronger seasonal cycle than the

261   molar fraction (Figure 2). The monthly mean value was -9.07‰ and -7.63‰ for January and

262   July, respectively, with a seasonal amplitude of 1.44‰. The mean value for the whole

263   experimental period was -8.48‰, which is slightly more negative than the MLO value (-

264   8.44‰). The summertime (June-August) $\delta^{13}C$ was 0.55‰ more enriched than the MLO

265   background value.

266   The strongest diurnal variation in the CO_2 molar fraction was observed in the autumn

267   season and the weakest in the winter season, with a diurnal amplitude of 27.9 ppm and 13.4

268   ppm, respectively (Figure 3). In the summer season, the peak value was observed at 07:00

269   and the lowest value at 19:00. Contrary to the CO_2 molar fraction, $\delta^{13}C$ showed the lowest

270   value in the early morning and the highest value in the afternoon in all the four seasons. The

271   diurnal amplitude was 1.36‰ in the summer and 0.66‰ in the winter.

272

273   **3.2 Isotopic composition of the surface sources ($\delta^{13}C_S$)**

274   Applying the Miller-Tans method and the Keeling plot to the whole experimental period

275   yielded an apparent source signature of -25.51±0.26‰ (mean ±95% confidence bound) for

276   sources in the YRD (Figure 4) and -25.99±0.21‰ for sources in Nanjing (Figure 5). Strictly,

277   neither method is valid over such an extensive period because the source signature varies

278   seasonally, violating the condition of constant source signal under which the methods can be

279   used. So Figures 4 and 5 are meant more as a data consistency check than for determining the

280   true annual mean source signatures.

281   During the two and a half years of observation, the monthly $\delta^{13}C_S$ was lower in the

282   winter and higher in the summer (Figure 6). The sources in the YRD had higher ^{13}C

283   compositions than those in in Nanjing. The January mean value (mean of January 2014 and

284   January 2015) was -24.13‰ and -24.66‰, and the mean value of the three August months

285   was -20.67‰ and -23.35‰ for the YRD and Nanjing, respectively. The mean value of the

286   whole observational period was -23.25‰ and -24.24‰ for the YRD and Nanjing,

287   respectively. These mean values based on the monthly analysis were 2.26‰ and 1.75‰

288   greater than the apparent source signatures derived from the application of the Miller-Tans

289   and the Keeling method to the whole dataset (Figures 4 and 5), respectively. The monthly

290    $\delta^{13}C_S$ for the YRD (Figure 6) was highly correlated with the monthly atmospheric $\delta^{13}C$

291   (Figure 2; linear correlation = 0.63, n = 30, p <0.001). The correlation between the monthly

292    $\delta^{13}C_S$ for Nanjing and the monthly atmospheric $\delta^{13}C$ was not as strong (linear correlation =

293   0.52, n = 30, p <0.01).

294   There appears to be some inter-annual variability in $\delta^{13}C_S$. In the YRD, the 12-month

295   mean $\delta^{13}C_S$ was -23.31‰ from March 2013 to February 2014 and -23.26‰ from March 2014

296   to February 2015. The atmospheric $\delta^{13}C$ also showed an increasing trend, from -8.36‰ in the

297   first period to -8.15‰ in the second period.

298

299   **3.3 Inventory data for anthropogenic sources**

300   In the YRD, coal combustion was by far the largest source of anthropogenic CO_2,

301   contributing 70% of the overall fossil-plus emission (Table 1). Here fossil-plus emission

302   includes contributions from combustion of all forms of fossil fuel and from non-cement

303   industrial processes. The second and third largest source were ammonia synthesis and pig

304   iron, with fractional contributions of about 9%. The fuel-plus source contribution to the total

305   anthropogenic emission was 91%, with the remaining 9% contributed by cement production

306   (Table 2).

307   In the Nanjing municipality, the fractional contribution of coal to the fossil-plus total was

308   52%, lower than that for the YRD, and the other three major sources were ammonia synthesis

309   (16%), pig iron (13%), and gasoline (11%). The fractional contribution of fuel-plus sources to

310   the total anthropogenic emission was 96.4% and the fractional contribution of cement

311   production was 3.6% (Table 1). The isotopic signature of the fossil-plus sources was 0.35‰

312   lower for Nanjing than for the YRD.

313   The overall effective isotopic signature of the anthropogenic sources weighted by the

314   source contributions was also lower for Nanjing than for the YRD (Table 2). The difference

315   was 1.76‰ and was a result of lower fractional contributions in Nanjing of coal combustion

316   and cement production, which have relatively high ^{13}C contents, and a higher fractional

317   contribution of natural gas, which is the fuel type with the lowest ^{13}C content.

318

319   **3.4. CO_2 fluxes in YRD and Nanjing**

320   The plant flux F_P obtained with the isotopic partitioning method for the YRD agreed with the

321   seasonal phenology expected for plants in this region (Figure 7). It was slightly negative in

322 the summer and positive in the winter, indicating net uptake and net release, respectively. The

323 annual mean plant flux for the calendar year 2014 was -0.01 mg $m^{-2}s^{-1}$. The net surface flux

324 F_S was 0.16 mg $m^{-2}s^{-1}$.

325   In Nanjing, the plant flux was positive throughout the year. This is because the

326 partitioning was done for the night hours when the natural ecosystems were a source of CO_2

327 due to autotrophic and heterotrophic respiration. The flux was greater in the summer than in

328 the winter (Figure 8). The annual mean plant flux for the calendar year 2014 was 0.06 mg $m^{-2}s^{-1}$

329 $^{2}s^{-1}$. The net surface flux was 0.18 mg $m^{-2}s^{-1}$.

330

4 Discussion

4.1 CO_2 molar fraction and $\delta^{13}C$ seasonality

333 The atmospheric CO_2 molar fraction observed in Nanjing showed very small seasonal

334 variation (summer versus winter difference of 7.9 ppm, July versus January difference of 15.6

335 ppm), in comparison with the data published for other cities. The CO_2 molar fraction

336 difference between the cold and the warm season is about 66 ppm in Phoenix, USA (Idso et

337 al. 2002). In Salt Lake City, USA, the CO_2 molar fraction in the summer is about 31 ppm

338 lower than in the winter (Pataki et al., 2003). In Chicago, USA, the CO_2 molar fraction varied

339 from 397 ppm in August 2011 to 427 ppm in January 2012, showing a seasonal amplitude of

340 30 ppm (Moore and Jacobson 2015). In Beijing, China, the seasonal variation of atmospheric

341 CO_2 molar fraction is about 64.5 ppm (August versus January; Pang et al. 2016).

342   Several factors contributed to the weak seasonality in Nanjing. The climate in the YRD

343 is relatively mild. The governmental energy policy prohibits winter heating in public

344   buildings. Most residential buildings also lack space heating in the winter. This is in contrast

345   to energy use patterns in northern cities. In London, UK, natural gas usage in the winter

346   heating season is 29% greater than in the non-heating autumn season (Helfter et al. 2011). In

347   Salt Lake City, USA, energy consumption in the winter was 41% greater than in the summer

348   (Bush et al, 2007). A similar seasonal trend of energy consumption has also been reported for

349   Beijing (Pang et al, 2016). In Chicago, natural gas usage varied 70% to 80% in winter and

350   about 50% in summer (Moore and Jacobson 2015). The weak energy use seasonality (Figure

351   2) partially explains why the observed CO_2 molar fraction had a smaller seasonal amplitude

352   than reported for other northern cities.

353   The weak seasonality of the observed molar fraction was also related to the low

354   vegetation cover in the YRD and in Nanjing. The forest cover ratio is about 35% in Nanjing

355   and in the YRD, and the overall he vegetation cover (forest plus other vegetation types) ratio

356   in the major cities in the YRD is lower than 45% (CESY, 2013; CSY, 2013). For comparison,

357   the vegetation cover ratio is 56% in Salt Lake City (Pataki et al. 2009) and 44% in Chicago

358   (Rose et al. 2003). Dense vegetation is known to deplete atmospheric CO_2 in the summer

359   season via photosynthetic uptake, amplifying the CO_2 seasonal amplitude.

360   Our $\delta^{13}C$ seasonal amplitude (January versus July difference 1.44‰) was 30 times the

361   amplitude observed at MLO (Figure 2) but agreed with those reported by most urban studies.

362   For comparison, the seasonal amplitude of $\delta^{13}C_a$ in Bangalore, India, was 0.89 to 1.32‰

363   (Guha and Ghosh 2015). Similar amplitudes have also been reported for Chicago (January

364   versus August difference 1.25‰; Moore and Jacobson, 2015) and Beijing (2.13‰; Pang et al.

365   2016). In Salt Lake City, the seasonal amplitude of $\delta^{13}C$ was approximately 1.6‰ because

366   much more natural gas consumption for heating in the winter than in the summer (Pataki et

367   al. 2006).

368

4.2 Influences of cement production on atmospheric $\delta^{13}C$

370   The high summer $\delta^{13}C$ was one of the most unique characteristics at our site. The midday

371     $\delta^{13}C$ reached -6.90‰ in July 2013 and -7.21‰ in August 2014, which were 1.57‰ and

372   1.11‰ higher than the MLO values. The highest monthly mean $\delta^{13}C$ occurred in July: -

373   7.44‰ in July 2013, -7.99‰ in July 2014 and -7.46‰ in July 2015. These values were -

374   1.03‰, -0.44‰ and -0.93‰ higher than the MLO value reported for the same months.

375   The high July values observed at our site cannot be fully explained by CO_2 removal by

376   plant photosynthesis. Photosynthesis and respiration are the two processes that dominate the

377   ^{13}C seasonality in plant-dominated landscapes, leading to higher $\delta^{13}C$ values in the summer

378   and lower values in the winter. In Park Falls, Wisconsin, USA, a site in a heavily-forested

379   landscape, $\delta^{13}C$ was -7.75‰ in August 2011 and -8.77‰ in February 2012 (Moore and

380   Jacobson, 2015). For comparison, $\delta^{13}C$ at MLO was -8.24‰ and -8.38‰ in these two

381   months. In other words, the photosynthetic effect raised the August $\delta^{13}C$ by 0.5‰ above the

382   background value, a smaller enrichment that observed at our site. Because of the low

383   vegetation fraction, the summer photosynthetic CO_2 uptake in YRD and Nanjing should be

384   lower than at Park Falls. According to the Carbon Tracker inversion analysis (Peters et al.

385   2007), the net ecosystem production at the grid point where Parks Fall is located is -0.22 mg

386     $m^{-2}s^{-1}$ in July but is only -0.13 mg $m^{-2}s^{-1}$ at the grid point corresponding to the YRD region.

387   We would expect from the photosynthetic effect alone that the summertime ^{13}C enrichment at

388   our site to be smaller, not greater than that observed at Parks Fall.

389   Furthermore, in a human-dominated landscape, the plant photosynthetic enhancement of

390   ^{13}C is offset by the CO_2 from fossil fuel combustion which has low ^{13}C contents. In Chicago,

391   the monthly δ^{13}C peaked in August at -8.29‰ during the calendar year 2011, which is 0.05‰

392   lower than the MLO for the same month. Similarly, in Beijing, the monthly δ^{13}C peaked at -

393   9.49‰ in August 2014, which is 1.17‰ lower than the MLO value for the same month.

394   We suggest that cement production was the factor responsible for the high δ^{13}C values in

395   the summer. The evidence supporting this interpretation is provided by data in Table 2 and

396   Figure 7. The δ^{13}C signal of anthropogenic CO_2 in the YRD would be -26.42‰ without

397   cement production and increased to -23.71‰ after inclusion of the cement source (Table 2).

398   This δ^{13}C value is much higher than those reported for other urban lands, such as -30.7‰ for

399   Los Angeles, USA (Newman et al. 2008) and about -31‰ for Salt Lake City, USA (Bush et

400   al. 2007). The overall surface source signal derived from atmospheric measurements (Figure

401   6, -23.25‰ and -24.24‰ for the YRD and Nanjing) was also more enriched than those

402   obtained from atmospheric measurements in other cities, such as -28.1±0.8‰ for Chicago in

403   August and September (Moore and Jacobson, 2015), -32.4‰ to -27.4‰ for Salt Lake City in

404   the growing season (Pataki et al. 2003), -27.0‰ for Beijing in the winter heating season

405   (Pang et al. 2016), and -29.3‰ for Los Angeles, USA (Newman et al. 2008).

406   The influence of cement production on atmospheric δ^{13}C has also been suggested for at

407   least two other urban sites. In Bangalore, India, δ^{13}C is 0.05‰ higher than that observed at an

408   island station in the Indian Ocean, and cement production in southern India (Guha and Ghosh

409 2015) is offered as a reason to explain the enrichment of urban δ^{13}C. The other urban site is

410 Beijing, China, where the δ^{13}C measurement may have been influenced by cement plants

411 outside the city (Ren et al. 2015, Pang et al. 2016).

412

413 **4.3 Net surface and plant fluxes in the YRD**

414 As a human-dominated landscape, the YRD was a net source of CO_2 on the monthly scale

415 even in the growing season (F_S, Figure 7). The seasonal trends of the net surface flux F_S and

416 the plant flux F_P were highly consistent with each other because the anthropogenic source

417 strengths were almost constant. The mean F_S between March 2013 and February 2015 was

418 0.17 mg m^{-2}s^{-1}, which consisted of 0.16 mg m^{-2}s^{-1} from fossil combustion and industrial

419 processes, 0.02 mg m^{-2}s^{-1} from cement production and -0.01 mg m^{-2}s^{-1} from biological

420 activities. The total anthropogenic CO_2 flux was 0.18 mg m^{-2}s^{-1} in the YRD, a 67% increase

421 from the value of 0.10 mg m^{-2}s^{-1} reported for 2009 (Shen et al. 2014). From 2009 to 2012, the

422 GDP increased by 56% according to the National Statistic Yearbook.

423 For comparison, we extracted the flux data from the Carbon Tracker database for the 9

424 pixels that cover the YRD region. The results show that the mean plant flux F_P is slightly

425 negative at -0.01 mg m^{-2}s^{-1} for 2012 (Peter et al. 2007). Our estimate of F_P for 2014 also

426 indicates that the region was a negligibly small biological sink of CO_2 (-0.009 mg m^{-2}s^{-1}).

427

428 **4.4 Comparison of the Miller-Tans and the Keeling method**

429 By applying the Miller-Tans and the Keeling plot method separately to the midday and

430 midnight periods, we obtained the effective source signatures that are consistent with the

431   inventory analysis for the YRD and for the Nanjing Municipality. The daytime Miller-Tans

432   method revealed that the sources were on average 1.01‰ more enriched in ^{13}C than the

433   signature $\delta^{13}C_S$ obtained with the nighttime Keeling plot analysis. For comparison, the overall

434     $\delta^{13}C_S$ of the anthropogenic sources in the YRD was also higher than that in Nanjing, the

435   difference being 1.76‰ (Table 2). The interpretation that the midday observations capture the

436   influence of surface sources in the YRD region is supported by a trajectory analysis and by an

437   analysis of the atmospheric methane to CO_2 emissions ratio observed at the same site (Shen

438   et al. 2014). We note that the atmospheric measurements gave a smaller difference between

439   the YRD and Nanjing than that obtained by the inventory data, likely because of different

440   biological contributions between the two spatial scales.

441   We argue that Keeling plot method is not appropriate for midday periods because the

442   surface air is influenced by both the surface sources and by entrainment of the background air

443   from above the boundary layer. If we applied the Keeling method to the midday observations,

444   the linear correlation coefficient was on average -0.898 which is weaker than the correlation

445   coefficient obtained with the Miller-Tans method (-0.956). The resulting mean $\delta^{13}C_S$ would

446   be 0.61‰ lower than the mean value shown in Figure 6. The difference in $\delta^{13}C_S$ between the

447   YRD (midday observations, Keeling method) and Nanjing (midnight observations, Keeling

448   method) would become too small (0.38‰).

449   Conversely, the Miller-Tans method is not recommended for midnight observations

450   because surface inversion conditions effectively prevent mixing of the free atmospheric air

451   with the surface air. If we applied the Miller-Tans method at monthly intervals to the

452   midnight data, the resulting $\delta^{13}C_S$ for Nanjing would increase to -23.72‰. For comparison,

453   the $\delta^{13}C_S$ for the YRD, obtained by applying the Miller-Tans method to the midday data, was

454   -23.25‰.

455

456   **5. Conclusion**

457   We showed that the temporal changes of $\delta^{13}C$ followed the seasonal patterns of

458   anthropogenic and biologic CO_2 emissions, with lower values in the winter than in the

459   summer. An unusual feature that has not been seen in other urban environment is that the $\delta^{13}C$

460   exceeded that at the Mauna Loa Observatory in some of the summer months. The highest

461   monthly ^{13}C was -7.44‰ observed in July 2013, which was 1.03‰ greater than the MLO

462   value for the same month. Evidence points to cement production as the key reason for why

463   the atmospheric $\delta^{13}C$ was higher than at the background site. In contrast to the ^{13}C signal, the

464   CO_2 molar fraction displayed very weak seasonality (July to January difference 15.6 ppm).

465   We hypothesized that the Miller-Tans method applied to the midday observations and the

466   Keeling plot method applied to the midnight observations should yield the effective isotopic

467   signature of surface sources at the regional (YRD) and the local (Nanjing) scale, respectively.

468   According to the Miller-Tans method, the effective source signal in the YRD was -25.51‰,

469   which was 0.48‰ higher than that in the Nanjing Municipality according to the Keeling plot

470   method. These results were consistent with inventory estimates of anthropogenic source

471   signatures at these two spatial scales.

472   By combining inventory data on anthropogenic C sources and the atmospheric

473   measurement of CO_2 molar fraction and its ^{13}C composition in an isotopic partitioning

474   framework, we inferred that natural ecosystems in the YRD were a negligibly small sink of

475   atmospheric CO_2, with an average flux of -0.009 mg m^{-2}s^{-1}. The Carbon Tracker inverse

476   analysis also reveals a small annual mean biological flux (-0.01 mg m^{-2}s^{-1}) for this region.

477

478   **Data availability:**

479   The atmospheric data are available upon request, from the Yale-NUIST Center website

480   http://yncenter.sites.yale.edu/publications or as an online data supplement to this paper.

481

482   **Acknowledgments:**

483   This research was supported by the National Natural Science Foundation of China (Grant

484   41475141, 41505005), the U. S. National Science Foundation (Grant 1520684), the Ministry

485   of Education of China (Grant PCSIRT), and the Priority Academic Program Development of

486   Jiangsu Higher Education Institutions (Grant PAPD). The first author also acknowledged a

487   visiting scholarship from China Scholarship Council and a Graduate Student Innovation

488   Grant from Jiangsu Provincial Government (Grant KYLX_0848).

References

Affek, H. P., Eiler, J. M. (2006). Abundance of mass 47 CO2 in urban air, car exhaust, and human breath. Geochimica et Cosmochimica Acta **70**(1): 1-12.

Akbari H, Menon S, Rosenfeld A. Global cooling: increasing world-wide urban albedos to offset CO2. Climatic Change, 2009, **94**(3-4): 275-286.

Andres, R. J., Marland, G., Boden, T., Bischof, S. (1994). Carbon dioxide emissions from fossil fuel consumption and cement manufacture, 1751-1991; and an estimate of their isotopic composition and latitudinal distribution, Oak Ridge National Lab., TN (United States);

Bai, Y., (2011) A comparative study on turbulent fluxes exchange over Nanjing urban and suburban in summer. (in Chinese) Nanjing, Nanjing University of Information Science & Technology.

Bi, J., Zhang, R., Wang, H., Liu, M.,Wu, Y. (2011). The benchmarks of carbon emissions and policy implications for China's cities: Case of Nanjing. Energy Policy **39**(9): 4785-4794.

Bowling, D. R., Sargent, S. D., Tanner, B. D., and Ehleringer, J. R. (2003). Tunable diode laser absorption spectroscopy for stable isotope studies of ecosystem–atmosphere CO2 exchange, Agric. Forest Meteorol. **118:** 1–19.

Bush, S. E., Pataki, D.E., Ehleringer, J.R. (2007). Sources of variation in δ13C of fossil fuel emissions in Salt Lake City, USA. Applied Geochemistry **22**(4): 715-723.

CESY (2013). China Energy Statistical Yearbook 2013: China Statistical Publishing House, Beijing. (in Chinese) Also available at: <http://www.stats.gov.cn/tjsj/ndsj/ 2013/indexch.htm>.

Clark-Thorne, S. T., C. J. Yapp (2003). Stable carbon isotope constraints on mixing and mass balance of CO2 in an urban atmosphere: Dallas metropolitan area, Texas, USA. Applied Geochemistry **18**(1): 75-95.

Coutts, A. M., Beringer, J., Tapper, N.J. (2007). Characteristics influencing the variability of urban CO2 fluxes in Melbourne, Australia. Atmospheric Environment **41**(1): 51-62.

CSY (2013). China Statistical Yearbook. National Bureau of Statistics of China. (in Chinese) Also available at: <http://www.stats.gov.cn/tjsj/ndsj/2013/indexch.htm>

Duan Y. (1995) Study of characteristics of coal isotope conposition in China Coal Geology & Exploration **23**(1) 29-33.

532   Ehleringer, J.R., Bowling, D.R., Flanagan, L.B., Fessenden, J.,Helliker, B., Martinelli, L.A.,
533   Ometto, J.P. (2002). Stable isotopes and carbon cycle processes in forests and grasslands.
534   Plant biology **4**(2): 181-189.

536   Farquhar, G., J. Lloyd (1993). Carbon and oxygen isotope effects in the exchange of carbon
537   dioxide between terrestrial plants and the atmosphere. Stable isotopes and plant carbon-water
538   relations **40**: 47-70.

540   Fessenden, J. E., J. R. Ehleringer (2002). Age-related variations in $\delta13C$ of ecosystem
541   respiration across a coniferous forest chronosequence in the Pacific Northwest. Tree
542   Physiology **22**(2-3): 159-167.

544   Friedman, L., A. P. Irsa (1967). Variations in isotopic composition of carbon in urban
545   atmospheric carbon dioxide. Science **158**(3798): 263-264.

547   Gorski G, Strong C, Good S P, Bares,R.,Ehleringer,J.R.,Bowen,G.J.. Vapor hydrogen and
548   oxygen isotopes reflect water of combustion in the urban atmosphere. Proceedings of the
549   National Academy of Sciences, 2015, **112**(11): 3247-3252.

551   Griffis, T. J., Lee, X., Baker, J.M., Sargent, S.D., King, J.Y. (2005). Feasibility of quantifying
552   ecosystem–atmosphere $C18O16O$ exchange using laser spectroscopy and the flux-gradient
553   method. Agricultural and Forest Meteorology **135**(1-4): 44-60.

555   Griffis, T J. (2013). Tracing the flow of carbon dioxide and water vapor between the
556   biosphere and atmosphere: A review of optical isotope techniques and their application.
557   Agricultural and Forest Meteorology, **174**:85-109.

559   Guha, T., P. Ghosh (2010). Diurnal variation of atmospheric $CO2$ concentration and delta C-
560   13 in an urban atmosphere during winter-role of the Nocturnal Boundary Layer. Journal of
561   Atmospheric Chemistry **65**(1): 1-12.

563   Guha, T. and P. Ghosh (2015). Diurnal and seasonal variation of mixing ratio and delta C-13
564   of air $CO2$ observed at an urban station Bangalore, India. Environmental Science and
565   Pollution Research **22**(3): 1877-1890.

567   Helfter, C., Famulari, D., Phillips, G.J., Barlow, J.F., Wood, C.R.,Grimmond, C.S.B., Nemitz,
568   E. (2011). Controls of carbon dioxide concentrations and fluxes above central London.
569   Atmospheric Chemistry and Physics **11**(5): 1913-1928.

571   ICLEI (International Council for Local Environmental Initiatives). (2008). Local government
572   operations protocol for the quantification and reporting of greenhouse gas emissions
573   inventories. [Available online at http://www.arb.ca.gov/cc/protocols/localgov/archive/final
574   lgo protocol 2008–09–25.pdf.]

575

Idso, S. B., Idso, C.D., Balling, R.C. (2002). Seasonal and diurnal variations of near-surface atmospheric CO 2 concentration within a residential sector of the urban CO 2 dome of Phoenix, AZ, USA. Atmospheric Environment **36**(10): 1655-1660.

Jasek, A., Zimnoch, M., Gorczyca, Z., Smula, E.,Rozanski, K. (2014). Seasonal variability of soil CO2 flux and its carbon isotope composition in Krakow urban area, Southern Poland. Isotopes in Environmental and Health Studies **50**(2): 143-155.

Keeling, C. D. (1958). The concentration and isotopic abundances of atmospheric carbon dioxide in rural areas. Geochimica et Cosmochimica Acta **13**(4): 322-334.

Keeling, C. D. (1961). The concentration and isotopic abundances of carbon dioxide in rural and marine air. Geochimica et Cosmochimica Acta **24**(3): 277-298.

Koerner, B., J. Klopatek (2002). Anthropogenic and natural CO2 emission sources in an arid urban environment. Environmental Pollution **116**: S45-S51.

Leavitt, S. W., Paul, E.A., Galadima, A.,Nakayama, F.S., Danzer, S.R., Johnson, H., Kimball, B.A. (1995). Carbon isotopes and carbon turnover in cotton and wheat FACE experiments. Plant and Soil **187**(2): 147-155.

Lichtfouse, E., Lichtfouse, M., Jaffrezic, A. (2003). delta C-13 values of grasses as a novel indicator of pollution by fossil-fuel-derived greenhouse gas CO2 in urban areas. Environmental Science & Technology **37**(1): 87-89.

Liu, H., Feng, J., Järvi, L., Vesala, T. (2012). Four-year (2006–2009) eddy covariance measurements of CO2 flux over an urban area in Beijing. Atmospheric Chemistry and Physics **12**(17): 7881-7892.

Lloyd, J., Kruijt, B., Hollinger, D.Y., Grace, J., Francey, R.J., Wong, S., Kelliher, F.M., Miranda, A.C., Farquhar, G.D., Gash, J.H.C. (1996). Vegetation effects on the isotopic composition of atmospheric CO2 at local and regional scales: theoretical aspects and a comparison between rain forest in Amazonia and a boreal forest in Siberia. Functional Plant Biology **23**(3): 371-399.

Lloyd, J., Francey, R.J., Mollicone, D., Raupach, M.R, Sogachev, A., Arneth, A., Byers, J.N., Kelliher, F.M., Rebmann, C., Valentini, R. (2001). Vertical profiles, boundary layer budgets, and regional flux estimates for CO2 and its 13C/12C ratio and for water vapor above a forest/bog mosaic in central Siberia. Global Biogeochemical Cycles **15**(2): 267-284.

McDonald, B.C., McBride, Z. C., Martin, E. W., Harley, R. A. High-resolution mapping of motor vehicle carbon dioxide emissions. Journal of Geophysical Research: Atmospheres, 2014, **119**(9): 5283-5298.

620 McManus, J. B., Zahniser, M.S., Nelson, D.D., Williams, L.R., Kolb, C.E. (2002). Infrared
621 laser spectrometer with balanced absorption for measurement of isotopic ratios of carbon
622 gases. Spectrochimica Acta Part A: Molecular and Biomolecular Spectroscopy **58**(11): 2465-
623 2479.

625 Miller, J. B., P. P. Tans (2003). Calculating isotopic fractionation from atmospheric
626 measurements at various scales. Tellus B **55**(2): 207-214.

628 Miller, J.B., Tans, P.P., White, J.W.C., Conway, T.J., Vaughn, B.W. (2003). The atmospheric
629 signal of terrestrial carbon isotopic discrimination and its implication for partitioning carbon
630 fluxes. Tellus B **55**(2): 197-206.

632 Moore J., Jacobson A.D. (2015). Seasonally varying contributions to urban CO_2 in the
633 Chicago, Illinois, USA region: Insights from a high-resolution CO_2 concentration and d13C
634 record. Elementa: Science of the Anthropocene **3**, 000052.

636 Mu, H., Li, H., Zhang, M., Li, M. (2013). Analysis of China's carbon dioxide flow for 2008.
637 Energy Policy **54**: 320-326.

639 Newman, S., Xu, X., Affek, H.P., Stolper, E., Epstein, S. (2008). Changes in mixing ratio and
640 isotopic composition of CO_2 in urban air from the Los Angeles basin, California, between
641 1972 and 2003. Journal of Geophysical Research **113**(D23) : 1-15.

643 NSY (2013). Nanjing Statistical Yearbook. Nanjing Municipal Bureau Statistics. (in Chinese)
644 Also available at: < http://www.njtj.gov.cn/2004/2013/renmin/index.htm>

646 Ometto, J. P., Flanagan, L.B., Martinelli, L.A., Moreira, M.Z., Higuchi, N., Ehleringer, J.R.
647 (2002). Carbon isotope discrimination in forest and pasture ecosystems of the Amazon Basin,
648 Brazil. Global Biogeochemical Cycles **16**(4):1-10.

650 Ometto, J.P., Ehleringer, J.R., Domingues, T.F., Berry, J.A., Ishida, F.Y., Mazzi, E., Higuchi,
651 N., Flanagan, L.B., Nardoto, G.B., Martinelli, L.A. (2006). The stable carbon and nitrogen
652 isotopic composition of vegetation in tropical forests of the Amazon Basin, Brazil.
653 Biogeochemistry **79**(1-2): 251-274.

655 Pang, J., Wen, X., Sun, X. (2016). Mixing ratio and carbon isotopic composition investigation
656 of atmospheric CO_2 in Beijing, China. Sci Total Environ **539**: 322-330.

658 Pataki, D. E. (2005). Can carbon dioxide be used as a tracer of urban atmospheric transport?
659 Journal of Geophysical Research **110**(D15102) : 1-8.

661 Pataki, D. E., Bowling, D.R., Ehleringer, J.R. (2003). Seasonal cycle of carbon dioxide and
662 its isotopic composition in an urban atmosphere: Anthropogenic and biogenic effects. Journal
663 of Geophysical Research-Atmospheres **108**(D23) : 1-8.

664

665 Pataki, D. E., Bowling, D.R., Ehleringer, J.R., Zobitz, J.M. (2006). High resolution
666 atmospheric monitoring of urban carbon dioxide sources. Geophysical Research Letters
667 **33**(3) : 1-5.

668

669 Pataki, D. E., Ehleringer, J.R., Flanagan, L.B., Yakir, D., Bowling, D.R., Still, C.J.,
670 Buchmann, N., Kaplan, J.O., Berry, J.A. (2003). The application and interpretation of Keeling
671 plots in terrestrial carbon cycle research. Global Biogeochemical Cycles **17**(1): 1-14

672

673 Pataki, D. E., Lai, C., Keeling, C.D., Ehleringer, J.R. (2007). Insights from stable isotopes on
674 the role of terrestrial ecosystems in the global carbon cycle. Terrestrial Ecosystems in a
675 Changing World, Springer**:** 37-44.

676

677 Pataki,D.E., Emmi,P.C., Forster,C.B., Mills,J.I., Pardyjak,E.R., Peterson,T.R.,
678 Thompson,J.D., Dudley-Murphy,E., An integrated approach to improving fossil fuel
679 emissions scenarios with urban ecosystem studies. Ecological Complexity, 2009, **6**(1): 1-14.

680

681 Pataki, D. E., Xu, T., Luo, Y.Q., Ehleringer, J.R. (2007). Inferring biogenic and anthropogenic
682 carbon dioxide sources across an urban to rural gradient. Oecologia **152**(2): 307-322.

683

684 Peters,W., Jacobson,A.R., Sweeney,C., Andrews,A.E., Conway,T.J., Masarie,,K., Miller,J.B.,
685 Bruhwiler,L.M., Petron,G., Hirsch, A.I., Worthy,D.E., van der Werf,G.R., Randerson,J.T.,
686 Wennberg,P.O., Krol,M.C., Tans,P.P., An atmospheric perspective on North American carbon
687 dioxide exchange: CarbonTracker.Proceedings of the National Academy of Sciences, 2007,
688 **104**(48): 18925-18930.

689

690 Rella, C. (2011). Accurate stable carbon isotope ratio measurements with rapidly varying
691 carbon dioxide concentrations using the Picarro δ13C G2101-i gas analyzer, Picarro White
692 Paper. Picarro Inc.

693

694 Ren, L., Wang, W., Wang, J., Liu, R. (2015). Analysis of energy consumption and carbon
695 emission during the urbanization of Shandong Province, China. Journal of Cleaner
696 Production **103**: 534-541.

697

698 Rose L S, Akbari H, Taha H. Characterizing the fabric of the urban environment: a case study
699 of Greater Houston, Texas. Lawrence Berkeley National Laboratory, 2003.

700

701 Satterthwaite D. Cities' contribution to global warming: notes on the allocation of greenhouse
702 gas emissions. Environment and Urbanization, 2008, **20**(2): 539–549.

703

704 Shen, S., Yang, D., Xiao, W., Liu, S., Lee, X. (2014). Constraining anthropogenic CH4
705 emissions in Nanjing and the Yangtze River Delta, China, using atmospheric CO2 and CH4
706 mixing ratios. Advances in Atmospheric Sciences **31**(6): 1343-1352.

707

708   Song, T., Wang Y. (2012). Carbon dioxide fluxes from an urban area in Beijing. Atmospheric
709   Research **106**: 139-149.

711   Sun, B., Dilcher, D.L., Beerling, D.J., Zhang, C., Yan, D., Kowalski, E. (2003). Variation in
712   Ginkgo biloba L. leaf characters across a climatic gradient in China. Proceedings of the
713   National Academy of Sciences **100**(12): 7141-7146.

715   Takahashi, H. A., Konohira, E., Hiyama, T., Minami, M., Nakamura, T., Yoshida, N. (2002).
716   Diurnal variation of CO2 concentration, Delta C-14 and delta C-13 in an urban forest:
717   estimate of the anthropogenic and biogenic CO2 contributions. Tellus B **54**(2): 97-109.

719   Tans, P. (1981). 13C/12C of industrial C02. In SCOPE 16: Carbon Qcle Modelling (B.Bolin,
720   ed.), John Wiley and Sons, Chichester, England, 127-129.

722   Thoning, K. W., Tans, P.P., Komhyr, W.D. (1989). Atmospheric carbon dioxide at Mauna Loa
723   Observatory: 2. Analysis of the NOAA GMCC data, 1974–1985. Journal of Geophysical
724   Research: Atmospheres (1984–2012) **94**(D6): 8549-8565.

726   Wada, R., Nakayama, T., Matsumi, Y., Hiyama, T., Inoue, G., Shibata, T. (2011). Observation
727   of carbon and oxygen isotopic compositions of CO2 at an urban site in Nagoya using Mid-IR
728   laser absorption spectroscopy. Atmospheric Environment **45**(5): 1168-1174.

730   Wang, W. , D. E. Pataki (2012). Drivers of spatial variability in urban plant and soil isotopic
731   composition in the Los Angeles basin. Plant and Soil **350**(1-2): 323-338.

733   Wen, X. F., Meng, Y., Zhang, X., Sun, X., Lee, X. (2013). Evaluating calibration strategies
734   for isotope ratio infrared spectroscopy for atmospheric $^{13}CO_2/^{12}CO_2$ measurement.
735   Atmospheric Measurement Techniques Discussions **6**(1): 795-823.

737   Widory, D. (2006). Combustibles, fuels and their combustion products: A view through
738   carbon isotopes. Combustion Theory and Modelling **10**(5): 831-841.

740   Widory, D., M. Javoy (2003). The carbon isotope composition of atmospheric CO2 in Paris.
741   Earth and Planetary Science Letters **215**(1-2): 289-298.

743   Yakir, D., L. da SL Sternberg (2000). The use of stable isotopes to study ecosystem gas
744   exchange. Oecologia **123**(3): 297-311.

746   Yang, H.M., Wang, H.Z. , Wu, Y.B. (2011). Observation and characteristics analysis of traffic
747   flow in Nanjing. (in Chinese) Environmental Science and Technology **24**(2): 98-101.

749   Zimnoch, M., Florkowski, T., Necki, J., Neubert, R. (2004). Diurnal variability of delta C-13
750   and delta O-18 of atmospheric CO2 in the urban atmosphere of Krakow, Poland. Isotopes in
751   Environmental and Health Studies **40**(2): 129-143.

752

753 Zobitz, J. M., Burns, S.P., Reichstein, M., Bowling, D.R. (2008). Partitioning net ecosystem
754 carbon exchange and the carbon isotopic disequilibrium in a subalpine forest. Global Change
755 Biology **14**(8): 1785-1800.

756

757 Zondervan, A., H. A. Meijer (1996). Isotopic characterisation of CO_2 sources during regional
758 pollution events using isotopic and radiocarbon analysis. Tellus B **48**(4): 601-612.

759

760   **List of Figure Captions**

761

762   Figure 1. Dependence of the observed $\delta^{13}C$ on the H_2O molar fraction. The lines represent

763   Equation 2b. Error bars are $\pm$ one standard deviation.

764

765   Figure 2. Monthly total CO_2 (upper panel) and $\delta^{13}C$ (lower panel). The solid line with cycle, dash

766   line with up triangles: midday (10:00-16:00) means; dashed line with down triangles, midnight

767   (22:00-6:00) means; smooth solid line stands, monthly means observed at the Mortgage Loan

768   Origination (MLO).

769

770   Figure 3. Mean diurnal variation of the CO_2 molar fraction (upper panels) and the $\delta^{13}C$ value

771   (bottom panels).

772

773   Figure 4. Application of the Miller-Tans method to all valid midday (10:00-16:00) data

774   obtained between March, 2013 and August, 2015. Each data point is one hourly mean. The

775   solid line is the geometric mean regression according to Equation 1.

776

777   Figure 5. Application of the Keeling mixing line method to all valid midnight (22:00-6:00)

778   data obtained between March, 2013 and August, 2015. Each data point is one hourly mean.

779   The solid line is the geometric mean regression according to Keeling plot

780

781 Figure 6. Time series of monthly ^{13}C signature of surface sources in the YRD obtained with

782 the Miller-Tans method (black line) and that in Nanjing obtained with the Keeling plot

783 method (grey line). The error bars are $\pm$ one standard deviation.

784

785 Figure 7. Time series of monthly net surface CO_2 flux (F_S), plant CO_2 flux (F_P),

786 anthropogenic CO_2 flux excluded cement emission (F_F) and cement CO_2 flux (F_c) in the

787 YRD. All the fluxes are in mg m^{-2}s^{-1}.

788

789 Figure 8. Time series of monthly net surface CO_2 flux (F_S), plant CO_2 flux (F_P),

790 anthropogenic CO_2 flux excluded cement emission (F_F) and cement CO_2 flux (F_c) in the

791 Nanjing. All the fluxes are in mg m^{-2}s^{-1}.

792

793

794 **Figure 1**. Dependence of the observed $\delta^{13}C$ on the H_2O molar fraction. The lines represent

795 Equation 2. Error bars are $\pm$ one standard deviation.

796
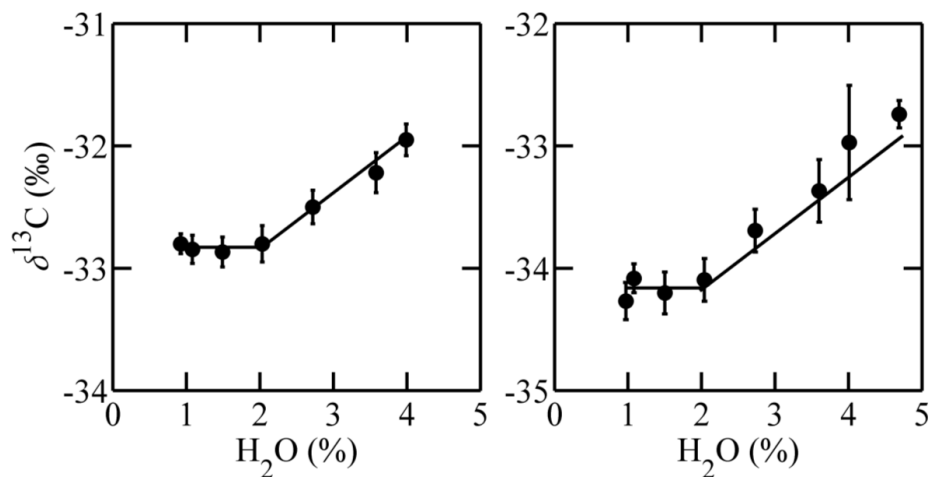
797

798   **Figure 2.** Monthly total CO_2 (upper panel) and $\delta^{13}C$ (lower panel). The solid line with cycle, dash

799   line with up triangles: midday (10:00-16:00) means; dashed line with down triangles, midnight

800   (22:00-6:00) means; smooth solid line stands, monthly means observed at the Mortgage Loan

801   Origination (MLO).

802
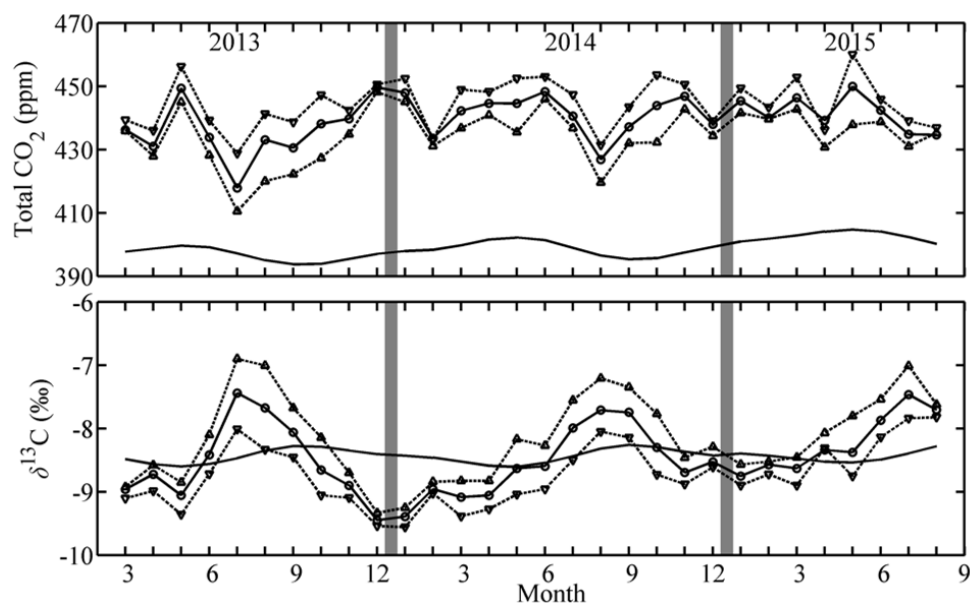
803
804

805   **Figure 3**. Mean diurnal variation of the CO_2 molar fraction (upper panels) and the $\delta^{13}C$ value

806   (bottom panels).
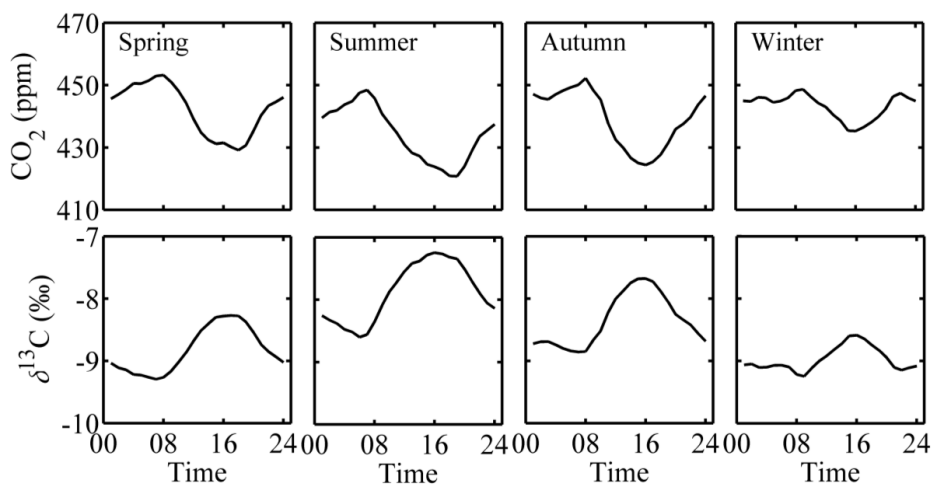
807
808

809   **Figure 4**. Application of the Miller-Tans method to all valid midday (10:00-16:00) data

810   obtained between March, 2013 and August, 2015. Each data point is one hourly mean. The

811   solid line is the geometric mean regression according to Equation 1.
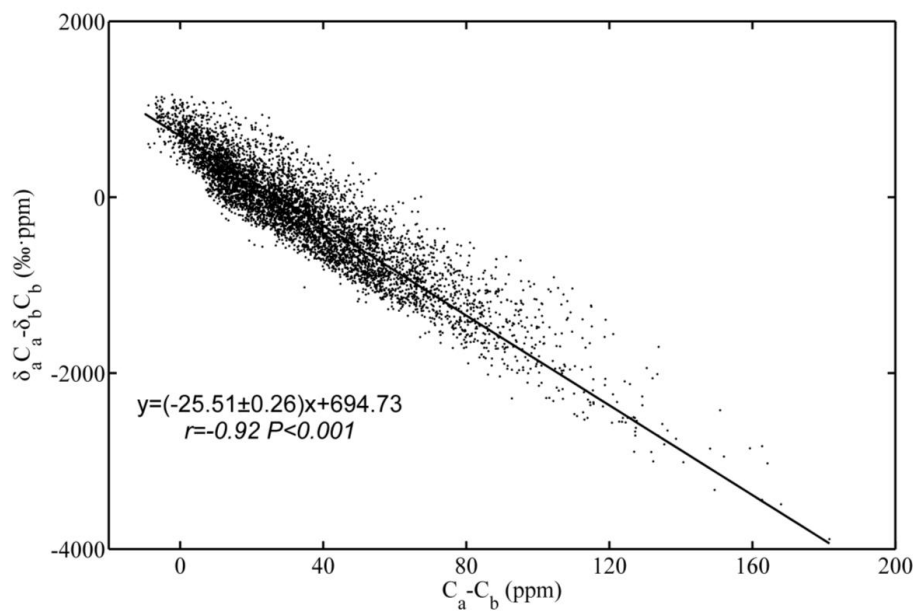
812

813

814 **Figure 5**. Application of the Keeling mixing line method to all valid midnight (22:00-6:00)

815 data obtained between March, 2013 and August, 2015. Each data point is one hourly mean.

816 The solid line is the geometric mean regression according to Keeling plot.
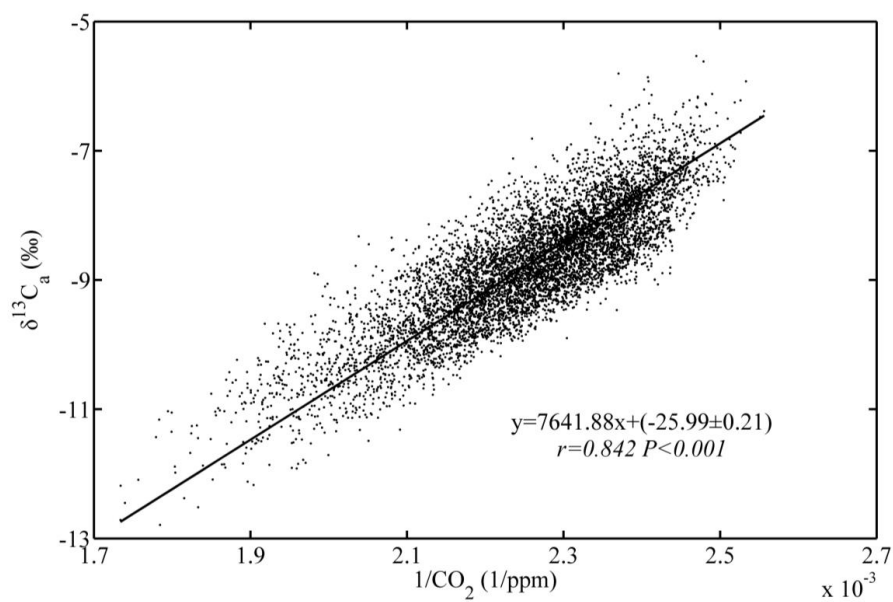
817

818

819 **Figure 6**. Time series of monthly ^{13}C signature of surface sources in the YRD obtained with

820 the Miller-Tans method (black line) and that in Nanjing obtained with the Keeling plot

821 method (grey line). The error bars are ± one standard deviation.
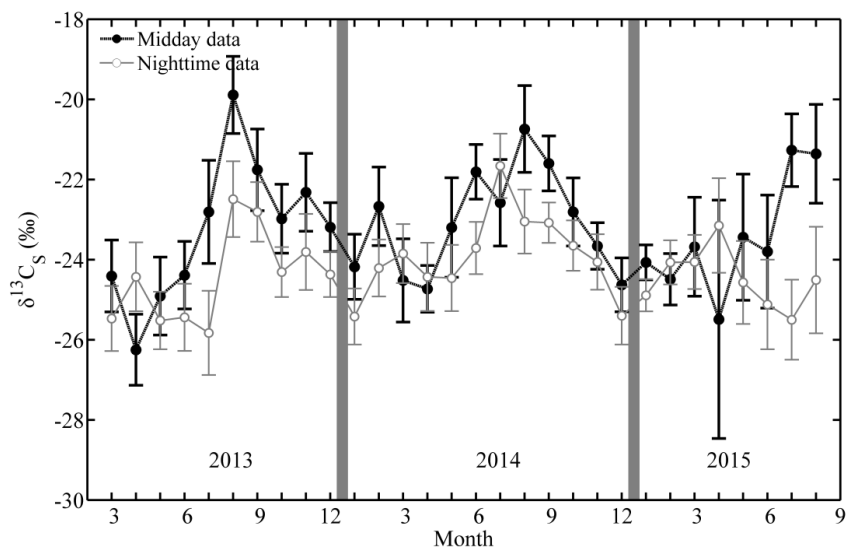
822

823

824   **Figure 7**. Time series of monthly net surface CO_2 flux (F_S), plant CO_2 flux (F_P),

825   anthropogenic CO_2 flux excluded cement emission (F_F) and cement CO_2 flux (F_c) in the

826   YRD. All the fluxes are in mg $m^{-2}s^{-1}$.

827
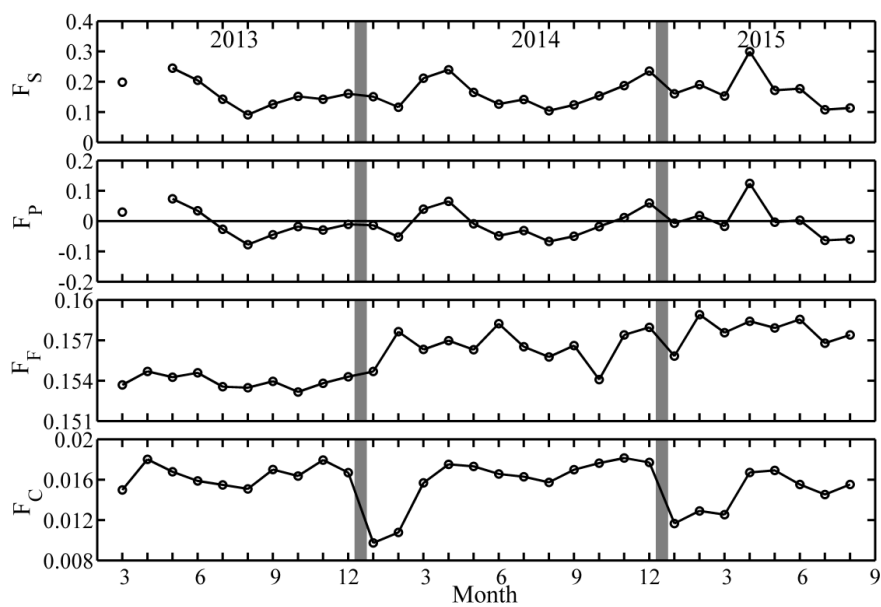
828

829

830 **Figure 8**. Time series of monthly net surface CO_2 flux (F_S), plant CO_2 flux (F_P),

831 anthropogenic CO_2 flux excluded cement emission (F_F) and cement CO_2 flux (F_c) in the

832 Nanjing. All the fluxes are in mg m^{-2}s^{-1}.
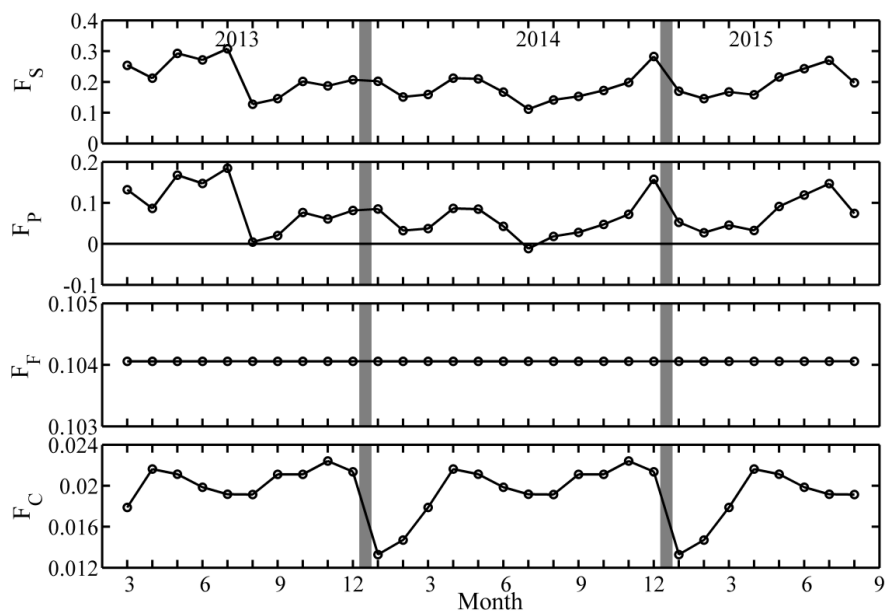
833

834

835   **Table 1**. Percentage of fossil plus sources and their δ^{13}C values for the YRD and Nanjing.

	Percentage (%)		δ^{13}C (‰)		
Sources	YRD	Nanjing	YRD	Nanjing	References
Coal	70.0	52.3	-25.46	-25.46	Duan 1995, Widory 2006
Gasoline	2.1	11.4	-28.80	-28.80	Widory and Javoy 2003
Diesel	3.2	1.6	-29.80	-29.80	Widory 2006
Fuel oil	2.1	0.3	-28.93	-28.93	Widory and Javoy 2003
Natural gas	2.7	5.0	-39.50	-39.50	Pang et al. 2016
LPG	0.7	0.2	-31.70	-31.70	Widory 2006
Pig iron	8.7	12.7	-24.58	-24.58	this study
Crude steel	1.5	0.7	-24.82	-24.82	this study
Ammonia synthesis	9.0	15.9	-28.50	-28.50	this study
Total	100	100	-26.07	-26.42	

836

837 **Table 2**. The isotopic composition of surface CO_2 sources and their percentage of

838 contribution in the YRD and Nanjing.

Sources	YRD		Nanjing	
	$\delta^{13}C$ (‰)	Percentage (%)	$\delta^{13}C$ (‰)	Percentage (%)
Fossil plus	-26.07	91.0	-26.42	96.4
Cement	0.20	9.0	0.20	3.6
Anthropogenic	-23.71	100	-25.47	100
Plant	-28.2	——	-28.2	——

839